ELSEVIER

Chemical Geology 243 (2007) 205–224

CHEMICAL GEOLOGY
INCLUDING
ISOTOPE GEOSCIENCE

www.elsevier.com/locate/chemgeo

Radioactive production and diffusional loss of radiogenic ^{40}Ar in clays in relation to its flux to the atmosphere

Abraham Lerman [a,*], Brandon M. Ray [a], Norbert Clauer [b]

[a] *Department of Earth and Planetary Sciences, Northwestern University, Evanston, Illinois, USA*
[b] *Centre de Géochimie de la Surface, CNRS et Université Louis Pasteur, Strasbourg, France*

Received 13 October 2006; received in revised form 26 March 2007; accepted 16 May 2007

Editor: D. Rickard

Abstract

This paper addresses the release mechanisms of radiogenic ^{40}Ar from clays, for the purpose of estimating the ^{40}Ar flux from the sedimentary crust to the atmosphere. Clays from sedimentary sequences of Cambrian to Neogene age show discrepancies between their depositional stratigraphic ages and the K–Ar apparent ages or dates of the different size fractions. The possible geochemical mechanisms that may be responsible for the K–Ar dates being either higher or lower than the stratigraphic age are discussed. In general, the known observation of a decrease in the K–Ar apparent age of clays with decreasing particle size is interpreted as due to a faster escape of radiogenic ^{40}Ar from the smaller particles. In the younger, Neogene clays, the mass fractions of ^{40}Ar lost are in a range from 13 to 34% in the fine-size particles that are smaller by a factor of 10 in their linear dimension than the bigger particles. In the older formation samples, Cambrian to Triassic, the ^{40}Ar loss is smaller, from 7 to 19%, for the same particle-size range. This smaller decrease in the $^{40}Ar/^{40}K$ ratio in the stratigraphically older samples may be, at least in part, accounted for by the closure of the mineral system after the process of ^{40}Ar escape went on for some time. In all sediments, a lowering of the K–Ar apparent age of the different size fractions, mainly in the smaller, is possibly due to authigenesis of mixed-layered illite–smectite and illite as a new generation of particles that result from, and are therefore better adapted to, the new diagenetic environment. In a Neogene basin sediments of depositional age <18 Ma, the amount of the authigenic illite fraction increases with an increase of its crystallization age from about 22 to 38%. If the rate of new crystallization is linear with time, this change corresponds to about 1.5%/Ma of authigenic particles added to the smaller-size fractions.

As an overall model, we present a mechanism that explains the lowering of the $^{40}Ar/^{40}K$ ratio and K–Ar apparent age in fine-clay size fractions based on the production of ^{40}Ar in a closed system for some period of time, followed subsequently by the diffusional escape of ^{40}Ar with its continuing production from ^{40}K in the particles. This analysis gives ^{40}Ar diffusion coefficients consistently in a range from 10^{-28} to 10^{-27} cm^2/s. From the results in this paper, the flux of radiogenic ^{40}Ar from the sedimentary crust to the atmosphere is estimated as 5 to 13×10^6 mol/year, which is about 15 to 40% of the flux from the whole continental crust, as reported by other investigators.

Keywords: Radiogenic ^{40}Ar production; Diffusion; Flux from sediments; Clay minerals; Authigenesis

1. Introduction

The $^{40}Ar/^{40}K$ ratios and K–Ar apparent ages of clay particles that are younger than their stratigraphic ages

* Corresponding author. Tel.: +1 847 4913238; fax: +1 847 4918060.
E-mail addresses: alerman@northwestern.edu (A. Lerman), nclauer@illite.u-strasbg.fr (N. Clauer).

0009-2541/$ - see front matter © 2007 Elsevier B.V. All rights reserved.
doi:10.1016/j.chemgeo.2007.05.014

have often been interpreted as a result of loss of radiogenic ^{40}Ar forming from ^{40}K, making the sedimentary lithosphere conceivably one of the sources of atmospheric argon. Because the radiogenic K–Ar ages of minerals may differ from their stratigraphic (depositional) age, the former are referred to as apparent ages or dates, as suggested by Faure (1986). Many authors have treated the ^{40}Ar loss from minerals without taking into account the continued production of ^{40}Ar during its escape from mineral particles (e.g., Lerman and Clauer, 2005, with references to others' work). This is a well-accepted practice in laboratory experiments or in those geologic environments where the duration of ^{40}Ar escape is known to be much shorter than the decay half-life of ^{40}K (1.24×10^9 years). However, because the $^{40}Ar/^{40}K$ ratios of clays in diverse sedimentary sequences often provide K–Ar apparent ages of 10^8 years (Fig. 1), the continuous production of ^{40}Ar cannot be disregarded if the duration of its escape extends to 10^7 to 10^8 years. In addition, the problem of simultaneous production and loss of radiogenic ^{40}Ar as a non-steady-state process on a limited scale was discussed earlier (Lerman and Clauer, 2005). In models of diffusional loss of ^{40}Ar from mineral particles of different geometric shapes, without taking into account its additional production (Turner, 1968; Dodson, 1973; Huon et al., 1993; McDougall and Harrison, 1999; Clauer et al., 2003), the mean diffusion coefficient of ^{40}Ar can be estimated if the following parameters are known: (1) the initial ^{40}Ar concentration or $^{40}Ar/^{40}K$ ratio in the particles, (2) the geometric shape and dimensions of the particles, and (3) the duration of the ^{40}Ar escape. Because the start time of the ^{40}Ar loss and its geologic duration are usually not well-known in sedimentary formations, only the mass fractions of the initial ^{40}Ar lost from different particle-size fractions can be computed from the assumed or measured values of the diffusion coefficients, particle size, and assumed duration of the ^{40}Ar escape period. In this paper we address the following issues that relate to changes in the $^{40}Ar/^{40}K$ ratios and K–Ar ages of clays, especially in terms of Ar release from sediments and its transfer to the atmosphere:

(1) We discuss the mechanisms that are variably responsible for the changes in the $^{40}Ar/^{40}K$ ratios and K–Ar apparent ages of sediments acting as open systems, such as the production and diffusional escape of ^{40}Ar from mineral particles, a diagenetic addition of K, and a possible addition of ^{40}Ar to clay minerals.

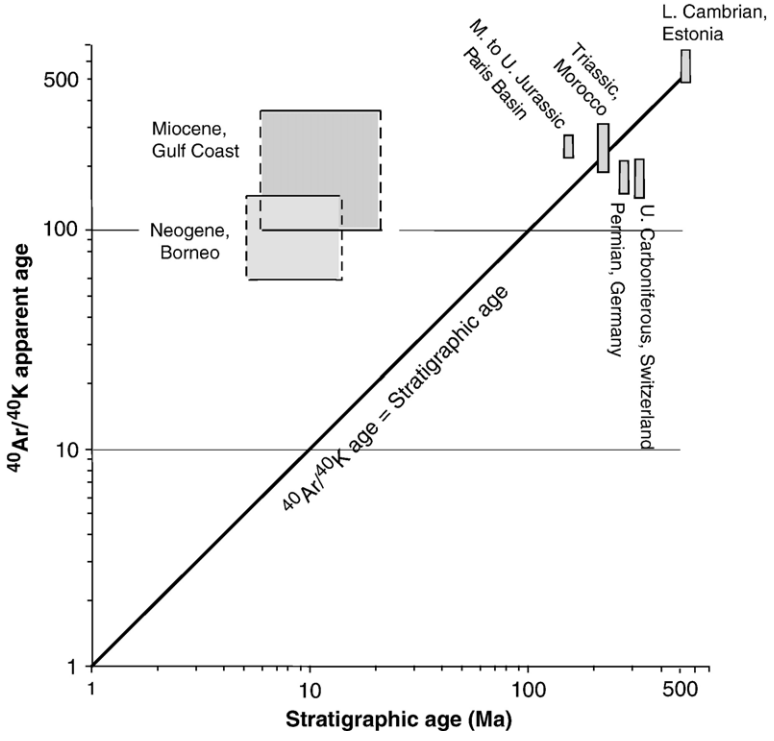

Fig. 1. Relationship between the $^{40}Ar/^{40}K$ ratios and K–Ar apparent ages of clays and the stratigraphic ages of their occurrences. Note the log–log scale of the two axes.

(2) We analyze published data on the $^{40}Ar/^{40}K$ ratios and K–Ar apparent ages of different particle-size fractions of clays from formations of different stratigraphic ages, where the samples show a greater ^{40}Ar loss from the smaller-size fractions. From these data, we estimate the fractions of radiogenic ^{40}Ar that were lost from the smaller particles. Although this interpretation is consistent with a generally accepted view of the relationship between the ^{40}Ar content and particle size (Faure, 1986), we also show that at least in some of the geologically younger formations, the K–Ar ages may be interpreted as due to an addition of K to some of the smaller particle-size fractions.
(3) We address a major issue of diffusional loss of ^{40}Ar from mineral particles and develop a new model that describes the ^{40}Ar production and loss. We apply this model to the sediment data of different ages and locations, where temperatures were likely not to exceed those of the upper range of illite stability, and estimate from it the diffusion coefficients of ^{40}Ar that consistently fall within a range of about one order of magnitude.
(4) Finally, from our results of the rates of ^{40}Ar loss from clay particles by different processes, we estimate the ^{40}Ar release rate from shales and compare it to some of the literature estimates of ^{40}Ar flux from the Earth's crystalline crust to the atmosphere.

The relationships between the stratigraphic ages and radiogenic $^{40}Ar/^{40}K$ ratios are not uniform, as shown in Fig. 1. The diagonal line in the figure represents the aging of clay particles acting as a closed system, initially free of ^{40}Ar, where the latter is produced by the decay of ^{40}K and neither ^{40}K nor radiogenic ^{40}Ar are added to, or lost from, the particles. The samples below the diagonal have apparent ages younger than their stratigraphic ages, indicating possible dominant losses of radiogenic ^{40}Ar in the course of their long geologic history since deposition, disregarding at this stage a possible addition of K, which might account for the same trend.

The clay samples that fall above the diagonal and, in particular, their larger-size fractions are older than their stratigraphic age, indicating that they had a long history before deposition as sediments. In particular, the clays in the stratigraphically younger sequences, such as the Miocene of the U. S. Gulf Coast and the Neogene of Borneo and East Slovak Basin (Clauer et al., 1997; Honty et al., 2004) have K–Ar apparent ages considerably older than their depositional age, inviting a speculation that relatively little ^{40}Ar degassing has occurred in such young sedimentary basins of ages <30 Ma. The plot in Fig. 1 agrees with the reported observation that some mineral fractions have $^{40}Ar/^{40}K$ ratios and K–Ar dates considerably older than the depositional stratigraphic age of the sediment (e.g., Glasmann et al., 1989, on older particles occurring in a Mesozoic sedimentary sequence). There are several possible major reasons behind the difference between the depositional stratigraphic age of the clays and their $^{40}Ar/^{40}K$ ratios, which will be discussed in the following sections.

2. Discrepancies between stratigraphic ages and K–Ar dates of clays

A $^{40}Ar/^{40}K$ date that is younger than the depositional age may indicate that (a) some of the radiogenic ^{40}Ar was lost from the particles, which is an interpretation favored by many investigators for clays in sedimentary environments, as well as for those affected by higher temperatures; or (b) potassium was added to some of the particle-size fractions in the course of diagenesis by the way of clay-particle neoformation in the small-size fractions that also contain older detrital core components next to which or on which the new authigenic material grew. However, although a K–Ar apparent age that is older than the depositional stratigraphic age likely indicates a pre-deposition history, it may also suggest that (c) the clays lost some of their K or, hypothetically, they lost relatively more ^{40}K than radiogenic ^{40}Ar during their post-depositional history, or (d) they acquired excess ^{40}Ar. The effects of relative losses or gains of ^{40}Ar and(or) ^{40}K on the $^{40}Ar/^{40}K$ ratio or the K–Ar apparent age of a mineral, t_{app}, are evident from an approximate relationship between the apparent age and the isotope atomic ratio in a potassium-bearing mineral that contained initially no ^{40}Ar, as given in Appendix A, Eq. (A.2b):

$$t_{app} \approx \frac{1}{\lambda_a}\frac{^{40}Ar}{^{40}K} \quad (1)$$

where $\lambda_a = 0.581 \times 10^{-10}$ year^{-1} is the ^{40}K decay rate constant to ^{40}Ar (Steiger and Jäger, 1977). For particles where the atomic ratio $^{40}Ar/^{40}K$ is 0.012 to 0.019 or smaller, the apparent age is up to 200 to 300 Ma, which makes t_{app} in Eq. (1) approximately a linear function of the isotope concentration ratio in that range, deviating by up to 5% to 8% from the more accurate value. The apparent age, t_{app}, depends only on the concentration ratio of the daughter ^{40}Ar and its parent ^{40}K. Thus, a

decrease in ^{40}Ar by a factor of 2, due to its release from the mineral particles (or an increase in ^{40}K by the same factor, due to its diagenetic addition), would lower the ratio and the apparent age also by a factor of about 2.

We shall address below the possible effects of processes (a)–(d).

2.1. Diffusional loss of ^{40}Ar

In Fig. 2, the diagonal line, labeled 1, represents a closed-system behavior, the K–Ar apparent age of which is the same as the depositional stratigraphic age, corresponding to the mineral particles that formed at the time of deposition. Diffusional loss of radiogenic ^{40}Ar from K-bearing minerals is generally believed to be a main mechanism of its escape. It has been extensively studied and discussed in the literature by many authors addressing such variable effects on the ^{40}Ar loss as higher temperatures due to burial or magmatic intrusions, mineral recrystallization, and regional tectonic deformation. As the decay of ^{40}K produces ^{40}Ca and ^{40}Ar, it may be recalled that the crystal ionic radius of K^+, 1.38 Å in a 6-fold coordination, is larger than that of Ca^{2+}, 1.00 Å (Shannon, 1976). The atomic radius of Ar is cited in the literature in a range from 0.71 to 1.88 Å, depending on the nature of the chemical bond, but Gaines (1958) gives a larger Ar radius in a K-mica as 2.16 Å, in comparison to the older value of the K^+ radius of 1.33 Å.

To assess a general effect of ^{40}Ar loss by diffusion across a particle surface, we use a model, given in Appendix A.2, that describes the production of ^{40}Ar from ^{40}K in a spherical particle, initially free of ^{40}Ar, and its diffusion out of the particle. As can be seen in the examples shown by curves 3 and 5 in Fig. 2, a true age of 150 Ma is lowered to about 105 Ma and 70 Ma, respectively, due to diffusional loss of ^{40}Ar from the particles at rates differing by a factor of about 5. It may be reiterated that the lowering of the $^{40}Ar/^{40}K$ ratio and the apparent age, t_{app}, in this calculated example is a net result of two processes: the ^{40}Ar production by decay of ^{40}K and the ^{40}Ar release by diffusion. A similarity of the results of a diffusional case to a case of K addition to particles is discussed in the next section.

2.2. Addition and removal of K in clay particles

The first, geologically short stage of K uptake by clays may be the cation exchange in transport of weathered materials by rivers to the ocean, where the monovalent ions (Na^+, K^+) show an increase over the exchangeable divalent ions in solids (Drever, 1997). In older sediments, addition of K to a small-size fraction (<0.1 μm) of clays in the Tertiary sediments of the U. S. Gulf Coast was

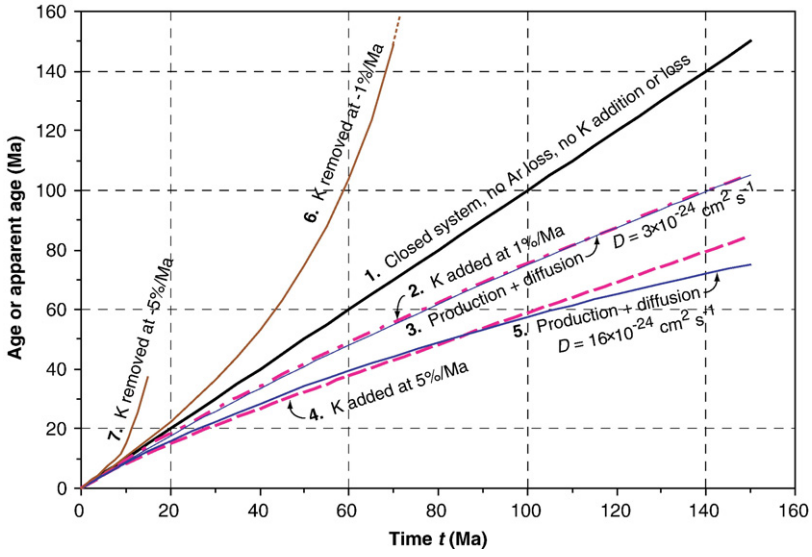

Fig. 2. Schematic changes in the K–Ar apparent age of clay minerals due to different mechanisms as a function of time. *1*: closed system, initially free of ^{40}Ar, where ^{40}Ar is produced by decay of ^{40}K, without any loss or addition of the parent and/or daughter isotope, Appendix A, Eq. (A.2a). *2*: addition of K to clay particles, initially free of ^{40}Ar, at a linear rate of +1%/Ma, no ^{40}Ar loss, Eq. (A.3). *3*: production of ^{40}Ar from ^{40}K in a spherical particle, of radius $r=10$ μm, initially free of ^{40}Ar, and loss of ^{40}Ar by diffusion with a diffusion coefficient $D=3.2\times10^{24}$ cm^2 s^{-1}, Eq. (A.9). *4*: addition of K as in 2, but at a higher linear rate of +5%/Ma, Eq. (A.3). *5*: production and diffusion of ^{40}Ar as in 3, but at a higher diffusion coefficient $D=15.8\times10^{24}$ cm^2 s^{-1}, Eq. (A.9). *6*: removal of K at a linear rate of −1%/Ma, same conditions as in 2, Eq. (A.3). 7: removal of K at a linear rate of −5%/Ma, same conditions as in 2, Eq. (A.3).

proposed by Aronson and Hower (1976) as a possible explanation of the lowering of the apparent age. Although the formation of new illite particles in a mixture with the older clay particles has been discussed by Clauer and Chaudhuri (1995, with references therein) and reported again by Clauer and Chaudhuri (2001), there are no sufficiently detailed data to identify and quantify a possible addition of K, in particular to different clay-particle sizes. In order to compare the calculated effects of ^{40}Ar loss by diffusion on the apparent age, t_{app}, of particles at a time scale of 150 Ma to possible effects of a diagenetic K addition to particles, curves 2 and 4 in Fig. 2 (calculated as given in Appendix A) show that the linear addition rates of K at +1%/Ma and +5%/Ma produce a similar lowering of the K–Ar apparent age as in the two hypothetical examples of diffusional loss. The similarity in itself of these results suggests that considerable caution needs to be exercised in the interpretation of the apparent ages within clay-particle assemblages where the smaller-size fractions show significantly younger K–Ar ages than the larger fractions. Such a case of the K addition to the smaller particles in an assemblage is discussed in Section 3.3.

A removal of K from illite or a mixed layered illite-smectite may, at least theoretically, lead to an increase in the K–Ar date of the clay minerals relative to their true age. An illustrative example of such an increase is shown by curves 6 and 7 in Fig. 2, for the two linear removal rates of K, similar in magnitude but of an opposite algebraic sign to those used for an addition of K, that is, −1%/Ma and −5%/Ma. However, as far as a removal of K is concerned, we are not aware of any data on a selective removal of K or ^{40}K from clay minerals, without affecting the radiogenic ^{40}Ar also contained in them in the interlayer sites.

2.3. Possible addition of ^{40}Ar to clay particles

Possible effects of addition of Ar gas, and the nuclide ^{40}Ar that is the most abundant Ar isotope (99.6 at.%) in the present-day atmosphere, on the K–Ar ages of clays is a little studied process. Preliminary experimental work (Clauer, 2005) indicates that limited amounts of radiogenic ^{40}Ar may occur in the argillite pore space and, not inconceivably, be adsorbed on mineral particle surfaces. Several argillite samples were successively kept evacuated for 1 week in a gas extraction line and the Ar extracted from the pore space had a ^{40}Ar/^{36}Ar ratio of 315±5, which is slightly but significantly beyond analytical uncertainty and higher than the atmospheric ratio of 295.5. Trapping of such Ar with a ^{40}Ar/^{36}Ar ratio slightly different from that of atmospheric Ar, is very difficult to detect on the K–Ar ages of authigenic minerals rich in K_2O, as illite-type clay particles commonly are, especially when older than 100 Ma. Also, a few ^{40}Ar/^{36}Ar ratios of modern oceanic sediments were reported to be slightly above the atmospheric reference value (Clauer, 2006).

Adsorption of Ar on grain surfaces of numerous human-made and natural materials is a well- and extensively studied field. However, such work using Ar and other gases in the determination of the solid surface area and pore-size distribution, is commonly done under the conditions that are very different from those of the sedimentary environment, at temperatures below or above the triple or boiling point of Ar (77 K to 90 K), and at the Ar partial pressures that range from that at the Ar boiling point ($p/p_{eq}=1$) to smaller values. Irrespective of the great temperature differences between the gas-adsorption experiments and the sedimentary environment, the partial pressure of Ar in the atmosphere is about 0.01 bar or 1/100 of the atmospheric pressure. Some of the authors report Ar volumes adsorbed on clays and other inorganic materials in the partial pressure range down to $p/p_{eq}<0.01$ to 0.1. At these values of Ar partial pressure, the amounts of Ar adsorbed on synthetic silica phases and synthetic zeolites of varying chemical composition and very different porosities, have been reported in the range from 10^{-4} to 10^{-3} mol Ar/g (Neimark, 2001; Saito and Foley, 1995; Thommes et al., 2006). On shungite or naturally occurring carbon black, adsorption of 1.8×10^{-4} mol/g was reported (Cascarini de Torre et al., 2004). On K-mica, Gaines and Rutkowski (1958) reported a decrease in adsorption with an increase in temperature from 77 K to 90 K, at p near 0.01 bar: adsorbed Ar mass decreased from 1.4×10^{-5} to 0.58×10^{-5} mol/g. On illite (Fithian illite), goethite, and gibbsite adsorption was 3.6×10^{-4} mol/g, and on a standard kaolinite (A.P.I.-5) it was 1.3×10^{-4} mol/g (Aylmore, 1974). The preceding values are very much higher than the ^{40}Ar concentrations encountered in clays and sedimentary K-feldspars: as shown by the data given in Section 5, ^{40}Ar concentration in a 600 to 300 Ma-old illite is of an order of magnitude 10^{-9} mol Ar/g, and in a K-feldspar of the same age it is 10^{-8} mol Ar/g. Clearly, the ^{40}Ar concentrations in sedimentary clay particles indicate that its occurrence there is not due to surface adsorption.

With regard to a possible uptake of Ar by clay particles from seawater or pore waters, we can make only some simplistic comparisons between the concentrations in clays and some natural waters, as we are not aware of any experimental studies of the Ar partitioning between aqueous solutions and clay minerals. As pointed out in the preceding paragraph, 10^{-9} mol Ar/g

is a concentration characteristic of clays of Early Phanerozoic age. Ar concentration in seawater and continental fresh waters falls in a range from about 11 to 18 μmol/kg or an average of about 1.5×10^{-8} mol Ar/g (Bachman et al., 2002; Biagi et al., 2004; Chen, 2006; Hamme and Emerson, 2004; Heaton and Vogel, 1981). In a sediment of a fairly characteristic porosity value of 25%, 1 cm^3 or 1 g of pore water is in contact with 3 cm^3 or about 7.5 g of solids. Thus if the mass of Ar in pore water were taken up by 7.5 g of clay, it would add about 2×10^{-9} mol Ar/g or nearly double the ^{40}Ar concentration in a 300 Ma-old illite, for which process there is no evidence. In fact, on the basis of groundwater studies in South Africa, Heaton and Vogel (1981) concluded that Ar concentrations have not been significantly modified by chemical reactions or radioactive decay within the aquifer.

3. ^{40}Ar loss from different particle-size fractions

3.1. K–Ar apparent age and particle size

In this section, we address the release of ^{40}Ar from the fine particle sizes of clayey sediments from formations of different ages, for which data were available. Some of the references to the geology and stratigraphy of the samples used in this study (Tables 1, B.1, B.2) are given in Lerman and Clauer (2005) and some in this paper. The geologic history and stratigraphic details of the sampled sites are discussed in the publications referenced for each sample. It should be noted that some of the sediments occur at depths and some are from surface outcrops. The depths of occurrence extend to approximately 5500 m in the U. S. Gulf Coast, suggesting in situ temperatures up to 180 °C (at an average geothermal gradient of 30 °C/km), which is within the upper limit of thermal stability field of illite of 270±30 °C (Hunziker et al., 1986; Hunziker, 1986). The decrease in the K–Ar apparent age with decreasing particle size of clays is a well-known phenomenon, discussed by many investigators. For samples of stratigraphic age ranging from the Lower Cambrian (Estonia) to the Upper Neogene (Borneo), the values of the K–Ar apparent age and ^{40}Ar/^{40}K ratio (R) as a function of the particle size (r) are shown in Fig. 3.

The analytical data in this figure are given in the Supplementary data, Appendix B. The linear regression lines plotted in the figure are:

$$\log R = b \log r + A, \quad (2)$$

where R is the ^{40}Ar/^{40}K atomic ratio, b is the slope, and A is the constant for each line as shown in the regression equations next to the lines. If a decrease in the ^{40}Ar/^{40}K ratio and K–Ar apparent age is due to the loss of ^{40}Ar

Table 1
Summary of ^{40}Ar diffusion coefficients in small-size clay particles, derived from the production and escape model, as explained in the text

Stratigraphic age, location, other data	Large size fraction (μm) and its apparent age (Ma)	Small-size fraction particle radius (μm) and apparent age (Ma)	Start time of ^{40}Ar loss in the model (<age of large size fraction)	^{40}Ar diffusion coefficient (10^{-27} cm^2 s^{-1})
Neogene, Borneo	6–40 μm, 100 Ma	0.05 μm, 70.4 Ma	50–95	0.2–3.2
Miocene U. S. Gulf	2–10 μm, 192 Ma	0.125 μm, 100 Ma	80–170	2.0–7.0
Coast, 5523 m		0.625 μm, 129 Ma	100–170	2.2–7.0
Same, 4417 m	2–10 μm, 266 Ma	0.125 μm, 137 Ma	150–250	1.7–13.9
		0.625 μm, 191 Ma	150–250	1.7–13.9
Same, 2331 m	2–10 μm, 336 Ma	0.125 μm, 165 Ma	150–315	1.3–9.2
		0.625 μm, 295 Ma	150–315	1.3–9.2
Same, 1582 m	2–10 μm, 358 Ma	0.125 μm, 164 Ma	250–340	2.2–13.0
		0.625 μm, 312 Ma	250–340	2.2–13.0
Upper Triassic, Keuper	0.4–2 μm, 217 Ma	0.05 μm, 146 Ma	100–200	0.1–0.6
Upper Triassic, Keuper	0.4–2 μm, 217 Ma	0.05 μm, 177 Ma	100–200	0.2–1.7
Upper Triassic, Keuper	0.4–2 μm, 217 Ma	0.15 μm, 163 Ma	100–200	0.5–3.0
Triassic, Morocco	10–20 μm, 315 Ma	0.1 μm, 224 Ma	200–300	0.4–3.5
Triassic, Morocco	10–20 μm, 315 Ma	0.1 μm, 209.5 Ma	200–300	0.4–3.2
Permian, Rotliegendes 4594.3 m	290 Ma (age 260–290 Ma)	0.05 μm, 166 Ma	150–270	0.2–0.9
Permian, Rotliegendes Mean of 4594.3 and 4657.7 m	275 Ma (age mid-point)	0.05 μm, 172 Ma	150–250	0.1–0.6

Detailed data are in Supplementary data, Appendix B, Table B.2.

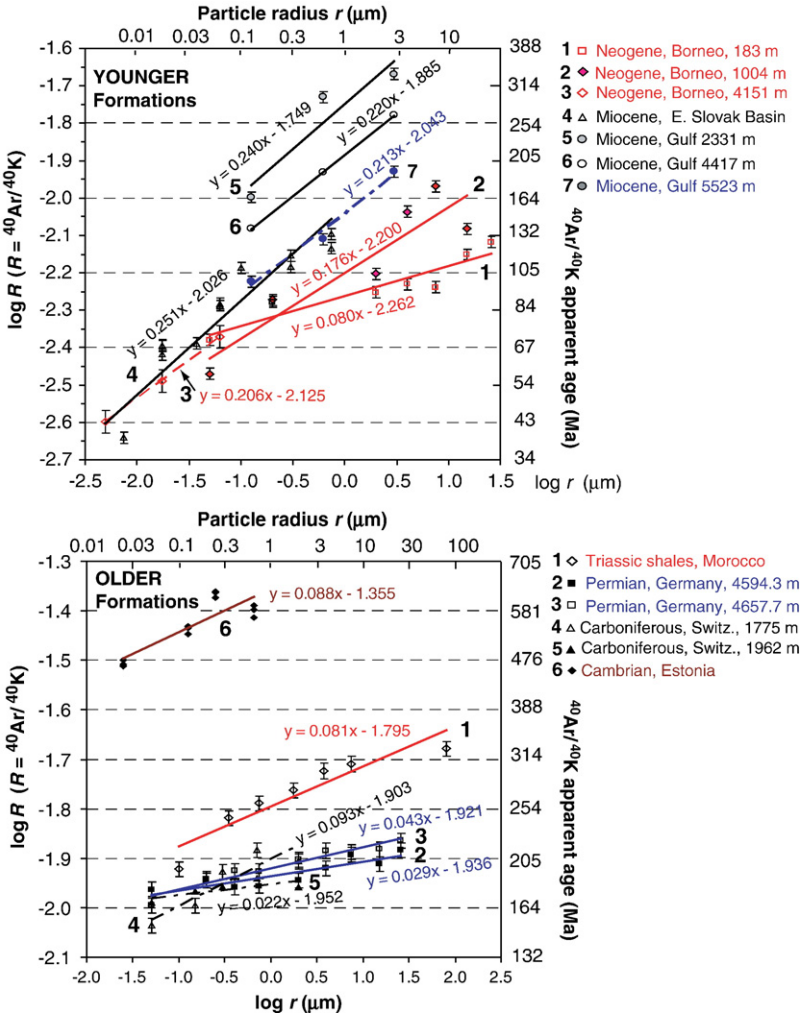

Fig. 3. Plots of the $^{40}Ar/^{40}K$ ratio (log R or y) as a function of the particle size (radius, log r or x) and linear regression lines in log–log coordinates. Note the differences in the vertical and horizontal scales of the plots of the younger and older formations. Data, regression line slopes, and intercepts are given in Appendix B, Table B.1. In the upper figure, the data of line 5 for a Gulf Coast, Miocene, sample from 2331 m depth are used in subsequent sections. The data of lines 1–3 (Neogene, Borneo, 183, 1004, and 4151 m depth) are also discussed in a later section.

from the minerals, then the fraction of ^{40}Ar that is lost from the smaller particles (radius r_1) relative to the larger particles (r_2) is:

$$f = 1 - R_1/R_2 = 1 - (r_1/r_2)^b. \quad (3)$$

The preceding relationship depends only on the slope of the logarithmic plot of the $^{40}Ar/^{40}K$ ratio as a function of the particle size, with the size ranging from the largest to smallest particles in the sample. It should be noted that the slopes of the Paleozoic and Mesozoic clays are as a whole less steep than those of the Neogene samples. Most of the Paleozoic and Mesozoic sample plots have slopes b in the range from about 0.03 to 0.09, whereas those of the Neogene samples from the U. S. Gulf Coast, Borneo, and East Slovak Basin, with the exception of one sample from the Neogene of Borneo, have slopes in the range from about 0.18 to 0.25 that also show a stronger decrease in the $^{40}Ar/^{40}K$ ratio and K–Ar apparent age with decreasing particle size. It should also be noted that the ages of the larger-size fractions in many of the Tertiary samples are as old as those of the Mesozoic and Paleozoic samples, likely reflecting their geologically long pre-depositional history. For a particle size decrease by a factor of 10 to 100 (r_1/r_2=0.1 to 0.01), from Eq. (3), the Paleozoic and Mesozoic smaller-size fractions have lost 7 to 19% of their ^{40}Ar for a particle size decrease by a factor of 10, and between 13 and 34% for a size decrease by a factor of 100. However, the Tertiary samples mentioned

above, would have lost 34 to 44% of the ^{40}Ar for a particle size decrease by a factor of 10, and the lost fraction would even be greater, 56 to 68%, for a 100-fold decrease in the particle size. The preceding results will be used for an estimate of the ^{40}Ar flux from sediments to the atmosphere in Section 5.

3.2. Changes in the slope of K–Ar age vs. particle size

As was discussed in Section 2, a decrease in the $^{40}Ar/^{40}K$ ratio and K–Ar apparent age of a clay particle may be due to either loss of ^{40}Ar or addition of ^{40}K to the existing particles due to the formation of new K-containing particles in some size fractions. However, it is difficult to account for a decrease in the apparent age with decreasing particle size as due to addition of K to the different size fractions. It should be noted that addition of ^{40}K to a clay particle would likely result in an increase of the particle mass from the addition of potassium, silica, alumina, and possibly other metals in approximately the same proportions as the stoichiometric chemical composition of the clay. An increase in particle mass by a factor of 2 has only a small effect on particle size: $2^{1/3}=1.26$ would be an increase factor in the radius of a spherical particle or of the linear dimension of a cubical particle. Such an increase is well within the range between the upper and lower limits of the size fractions that are usually reported as differing by a factor of 2 or more. Thus, an increase in particle size due to a diagenetic increase of mass may be disregarded.

The smaller slopes b (Fig. 3) in the older, Paleozoic and Mesozoic sediment samples may be due to the flattening of the slope in a system that lost some ^{40}Ar over some period of time and subsequently became closed, where ^{40}Ar continued to accumulate in the particles without loss. This flattening of the slope can be qualitatively accounted for by the difference between the concentration ratio $R_0=(^{40}Ar/^{40}K)_0$ values at the time of closure in the smaller and larger particles. An increase in the value of R with time in a closed system that contains initially some $R_0=(^{40}Ar/^{40}K)_0$ is (cf. Appendix A, Eq. (A.1)):

$$R = \frac{\lambda_a}{\lambda}\left(e^{\lambda t} - 1\right) + R_0 e^{\lambda t}. \quad (4)$$

Because the initial ratio in the smaller particles, $R_{0,1}$, is smaller than that in the larger particles, $R_{0,2}$ ($R_{0,1}<R_{0,2}$), a relative increase in the $^{40}Ar/^{40}K$ ratio in the smaller particles is greater than that in the larger ones:

$$R_1/R_{0,1} > R_2/R_{0,2}. \quad (5)$$

The latter relationship shows that the smaller particles, of a lower initial ratio $(^{40}Ar/^{40}K)_0$, "age" faster than the larger particles and an increase in log R over a period of time of, for example, 100 to 200 Ma, would be greater for the smaller particles than for the larger sizes, resulting in a flatter slope of the curve of log R vs. log r. Over such periods of time, a decrease in the slope steepness by a factor of 2 may occur. This, however, is only a qualitative indication of the direction of the slope change in a system that was open for some time and then became closed, as neither the time of closure nor the initial $^{40}Ar/^{40}K$ ratio is usually known.

3.3. Impact of particle nucleation during diagenesis

Among the Neogene clay samples beneath the Mahakam River delta in Eastern Borneo (Kalimantan), the deepest (4151 m), intermediate (1004 m), and shallowest (183 m) plotted in Fig. 3 (Table B.1), show different decrease patterns in the K–Ar apparent age with decreasing particle size: the slope of the apparent age vs. particle-size plot is pronouncedly less steep in the stratigraphically youngest sample at 183 m:

$$\begin{aligned}
&\text{At 183 m:} && \log R = 0.080 \log r - 2.262\\
&\text{At 1004 m:} && \log R = 0.176 \log r - 2.200\\
&\text{At 4151 m:} && \log R = 0.206 \log r - 2.125.
\end{aligned}$$

The Mahakam Basin is located in the area of the present-day Mahakam River delta (near S0.5°, E117°) and it has been receiving eroded products of the surrounding mountain terrains, of age between about 95 and 125 Ma (Furlan, 1994; Furlan et al., 1996). This material might have lost some Ar and K due to surface weathering of the source terrain. In the course of accumulation and progressive burial of the sediment, the loss of ^{40}Ar continued, as evidenced by the data shown in Fig. 3 and Table B.1, but it is difficult to ascertain whether any K continued to be lost from the larger particle fractions. However, an indication of the K addition to the smaller fractions at depths between 1000 and 4000 m is discussed below. Again, as suggested by Aronson and Hower (1976) and discussed at length by Clauer and Chaudhuri (1995), burial at about 4000 m not only induces loss of ^{40}Ar, but also addition of K, especially to the smaller-size fractions. In the case of the Mahakam Basin, illite size fractions of shales show a stepwise increase in K, from 0.34 wt.% at 800 m depth to 6.2 wt.% in the interval 3200–4500 m (Clauer et al., 2004). Considering a linear geothermal gradient of 30–40 °C/1000 m, the 4000-m burial induced a temperature increase of 140–180 °C, which is definitely in the upper

temperature range of illitization in volcanogenic sedimentary rocks (Šucha et al., 1993).

The older sample from 4151 m depth (Table B.1) occurs near the stratigraphic and seismological age marker of 18 Ma at 4000 m (Furlan et al., 1996; Clauer et al., 2004). Also, the K–Ar apparent age of the coarsest fraction in the deeper sample is comparable to that of the finer fractions in the upper samples. These differences in the three size fractions of the three samples suggest that the finest fractions (<0.02 and <0.2 μm) of the two deeper samples already contain newly-formed (authigenic) diagenetic illite particles. In principle, a detrital component may be expected to be older than a newly-formed authigenic particle, and a mixture of the two would have a younger apparent age than the detrital component alone. From the stratigraphic age of the deepest sample of 18 Ma, the stratigraphic age of the sample at 1004 m can only be estimated as being reasonably close to 4.5 Ma and the youngest sample at 183 m as close to 1 Ma. If the depositional age of the youngest sample at 183 m is too short and the burial too shallow, for a significant amount of authigenic illite and/or mixed-layered illite–smectite to have formed, the mineral neoformation probably started in the older samples about 4–5 Ma after the time of their deposition, which points to a temperature of about 60–70 °C that is considered to initiate illitization (Šucha et al., 1993). Therefore the regression line of the shallow sample at 183 m (Fig. 3) that is given above, may represent the apparent ages of the detrital clay particles in the older samples near the time of their deposition. Using this approach, the apparent age of the fine fraction (r=0.05 μm) in the 1004 m sample would be 72.6 Ma, as compared to the reported apparent age of 57.4 Ma. Similarly, for the stratigraphically older sample at 4151 m, the estimated apparent age of the smallest fraction (r=0.005 μm) would be 60.6 Ma, as compared to the reported age of 43 Ma; for the next size fraction (r=0.0175 μm), the apparent age would be 66.9 Ma, instead of the measured 54.9 Ma. The calculation of the authigenic and detrital mass fractions, given below, is based on an assumption that the age of authigenic illite in the sample that is now at 1004 m is about 4.5 Ma and about 18−4=14 Ma in the 4151 m sample. Realizing the very approximate nature of this reasoning, we may outline mass fractions of newly-formed illite (x) in the older samples to be reasonably close to the values given below.

$$\begin{aligned}
&\text{At 1004 m, } r = 0.05\ \mu\text{m}: && 4.5x + 72.6(1-x) = 57.4; && x = 22\%\\
&\text{At 4151 m, } r = 0.0175\ \mu\text{m}: && 14x + 66.9(1-x) = 54.9; && x = 23\%\\
&\text{At 4151 m, } r = 0.005\ \mu\text{m}: && 14x + 60.6(1-x) = 43; && x = 38\%.
\end{aligned}$$

From the above results, the rate of the authigenic illite formation is about 1.5%/Ma, if the rate were linear with time. Although the preceding results are only a crude approximation of a magnitude of possible neoformation of very fine-clay particles during burial diagenesis at a time scale of 10^6 years, they show that authigenesis was more extensive in the older and finer fractions, as may be expected, and ultimately they allow reasonable estimations of the mixtures of detrital and authigenic illite-type materials in shale rocks, depending on their combined K–Ar evolution, including ^{40}Ar production and diffusion, and ^{40}K release and addition, which has never been reported to the best of our knowledge.

A complete understanding of the mechanism of the ^{40}Ar loss and/or diagenetic addition of ^{40}K to different size fractions still requires more detailed information than is currently available, particularly on the mineralogical and chemical composition, and crystallographic characteristics of both the younger authigenic and older detrital clay particles depending on their location in progressively buried sedimentary formations. As the size fractions of young K–Ar apparent ages may be mixtures of older detrital and younger authigenic particles, it might be possible to separate the detrital from authigenic clays and determine their relative proportions similarly to the approximating procedure used earlier in this section, if the diagenetic processes at in situ environmental temperatures were known from independent experimental determinations.

4. Release and production of ^{40}Ar in fine particles

4.1. Conceptual model

The ^{40}Ar loss from minerals is generally viewed as a diffusional process and its analysis is based on the diffusion from particles of such model shapes as spheres, flakes, or cylinders, taking into account the local conditions of temperature and duration of the diffusional loss. As was mentioned in the Introduction (Section 1), the ^{40}Ar loss from minerals has often been treated without taking into account the continued production of ^{40}Ar during its escape from mineral particles. However, the continuous production of ^{40}Ar cannot be disregarded if its escape duration extends to 10^7 to 10^8 years. To take this into account, we use a model given in Appendix A.2. Conceptually, the simplest process is the production and simultaneous diffusional loss of ^{40}Ar since the formation of the particle to some future time, such as the present. We believe that a more realistic conceptual model is as follows:

(1) ^{40}Ar accumulates in clay particles at a rate close to that occurring in a closed system where the ^{40}Ar/^{40}K ratio and, consequently, the K–Ar apparent age increase;

(2) at some time, particles begin to lose ^{40}Ar by diffusion across the particle surface;
(3) both the ^{40}Ar that accumulated prior to the start of diffusional loss, and the ^{40}Ar that continues to be produced are lost from the particle by diffusion.

Thus in order to evaluate the ^{40}Ar flux out of the particles, their size and shape, and the diffusion coefficient should be known. In general, the $^{40}Ar/^{40}K$ is not known at the start of the diffusional loss nor is it known when diffusion started before the present or how long it did go on. The causes of the start of the loss, such as an increase in temperature, do not explicitly enter in the model. An important parameter is the particle shape that is known to affect the computed results in simpler ^{40}Ar diffusion models, where the continuous production of ^{40}Ar is not considered. Fig. 4A–C shows the separate and combined results of the three processes in a model calculation for spherical and flake-shaped particles. The particle is simulated as "a closed system" for the first 150 Ma, when the loss of ^{40}Ar begins (curve 1). The ^{40}Ar production continues from the ^{40}K concentration remaining at 150 Ma (curve 2). The combination of the two processes is shown in curve 3. For lengths of time of 50 Ma or more since the start of the diffusional loss, the continuing production of ^{40}Ar may add significantly to the $^{40}Ar/^{40}K$ ratio and it makes the K–Ar apparent age normally greater than in the case of the ^{40}Ar loss only. Two particle shapes are used in the illustration in Fig. 4: a sphere of diameter 2 μm and a flake or slab with a linear distance of 2 μm between the two parallel planes across which the diffusion occurs.

As expected, diffusion only across two planes of a flake removes less material from this particle shape than from a sphere, when the diffusion coefficient (D) and time (t) are the same in both, as shown in Fig. 4A,B. In particular, a flake in Fig. 4B shows a relatively strong increase in the K–Ar apparent age and $^{40}Ar/^{40}K$ ratio in comparison to the sphere, at the same value of D. To make the ^{40}Ar loss in a flake comparable to that in a sphere over the same period of time, the diffusion coefficient in the flake should be about 5 times greater, as shown in Fig. 4C. The particle shape has therefore a significant role in the interpretation of the K–Ar apparent ages and $^{40}Ar/^{40}K$ ratios. In models of ^{40}Ar loss from spherical particles or other shapes by diffusion without production, as given by Eqs. (A.4), (A.5), and (A.12) in Appendix A, the fraction of ^{40}Ar or any other non-reactive substance escaping from a particle is the highest for the sphere, followed closely by the cube, and it is the lowest for the flake or slab, where the three particle shapes are characterized by a fixed value of the diffusion coefficient D and a characteristic linear dimension r, that are combined in the dimensionless parameter Dt/r^2, (e.g., McDougall and Harrison, 1999, p. 141). In a sphere or cube, the outward diffusion takes place across the entire surface of the particle, but in a flake it takes place only across the two parallel planes or 1/3 of the surface of a cube of dimensions equal to those of a flake (Fig. 4). The choice of the sphere or flake as a model of a clay particle is clearly an approximation. In the monoclinic unit cell of illite or smectite (dimensions $a \approx 5$ Å, $b \approx 9$ Å, $c \approx 10$ Å, and unit cell volumes of 470 and 453 Å^3), K-atoms occupy the interlayer sites where ^{40}Ar is also produced and from where it may diffuse in the a- and(or) b-axis direction and, perhaps less likely, along the c-axis through the octahedral and tetrahedral layers. Significantly, the exchangeable cations in kaolinites have been reported as occurring not only on the basal surfaces but also on the particle edges (Sayed Hassan et al., 2005), and in a Na-smectite the lateral edge surface area was reported as accounting for about 11% of the total surface area (Tournassat et al., 2003). Thus, the choice of the sphere model for clay-particle shape may be considered as an upper limit, where diffusion is across the entire surface, and the flake model as a lower limit where diffusion is across two surfaces only.

4.2. Continuous production and loss of ^{40}Ar

The model of continuous production and loss of ^{40}Ar in particles containing no ^{40}Ar initially is given in Appendix A, Eq. (A.9). We demonstrate first a simple application of this model to a suite of Miocene clays before giving a more detailed and realistic analysis. Fig. 5 shows the curves of the K–Ar apparent ages, calculated using this model for spherical particles of radius $r = 0.125$, 0.21 to 0.64, and 3 μm, where they are compared to the apparent ages of two size fractions of clays from the Miocene of the U. S. Gulf Coast. The clay samples (Tables 1 and B.1), as studied and reported by Perry (1974), represent four depths in the sedimentary sequence, from 1582 to 5523 m, the estimated stratigraphic age range of which is from 23.3 Ma for the deepest sample to possibly as low as 5.2 Ma for the uppermost. As mentioned earlier, the largest size fraction, 2–10 μm range or 3 μm mean particle radius, has the highest $^{40}Ar/^{40}K$ ratios and oldest K–Ar apparent age in each sample, whereas the smaller fractions of 0.625 and 0.125 μm show lower ratios and younger apparent ages. Another characteristic of this suite of samples is that the shallowest sample of 1582 m depth has the oldest K–Ar apparent ages of 358 to 164 Ma, whereas the deepest sample from 5523 m has the youngest K–Ar apparent

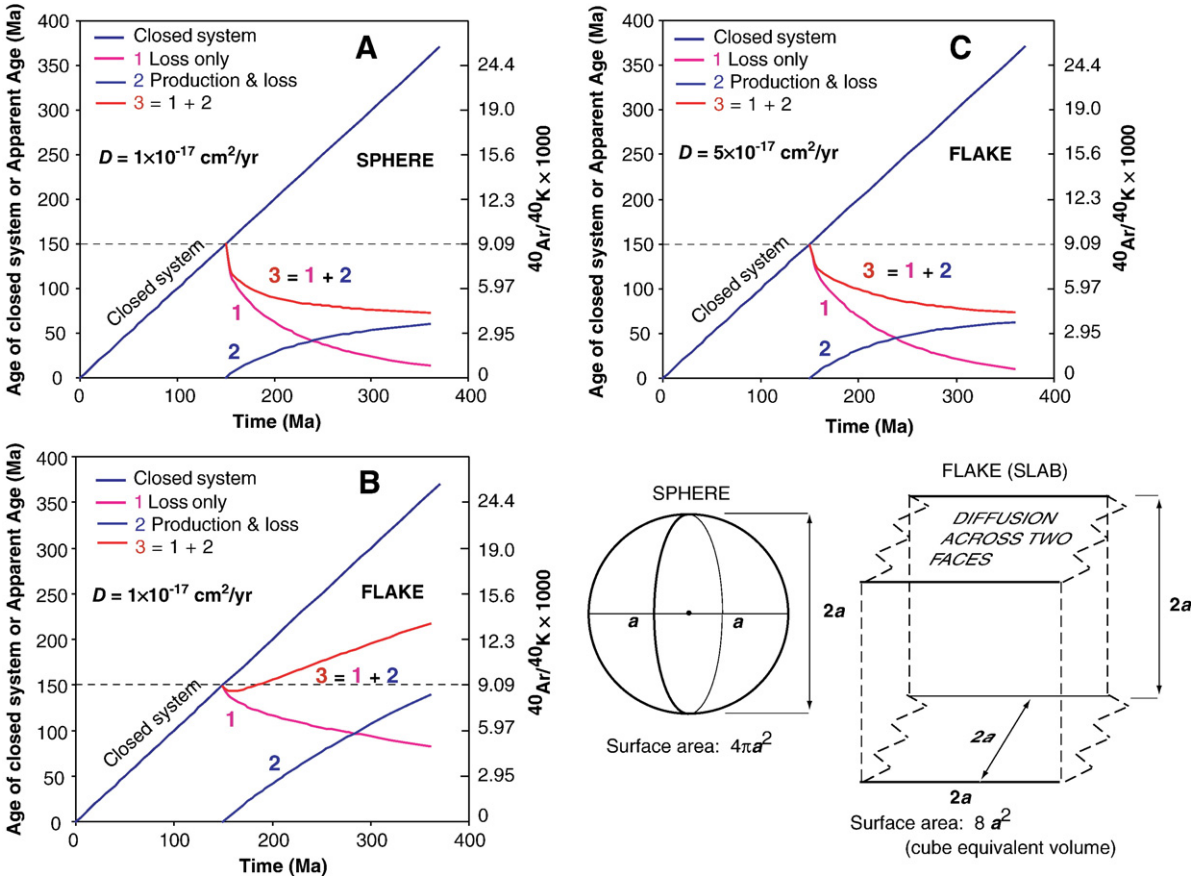

Fig. 4. Calculated $^{40}Ar/^{40}K$ ratios and K–Ar apparent ages of a sphere and a flake. Sphere diameter and flake thickness are the same ($2r$), $r=1$ μm. Model example: ^{40}Ar escape begins at a particle age of 150 Ma. Escape from a flake (B) is much slower than from a sphere (A) of the same dimensions. To attain the same apparent age or $^{40}Ar/^{40}K$ ratio in a flake as in a sphere, the diffusivity of ^{40}Ar in a flake should be about 5 times greater (C). Discussion in the text. Sphere: curve 1 calculated from Eq. (A.5), Appendix A; curve 2, Eq. (A.9); curve 3, Eq. (A.11). Flake or slab: curve 1, Eq. (A.12); curve 2, Eq. (A.13); curve 3, Eq. (A.14).

ages of 192 to 100 Ma. Here, burial reduced the K–Ar apparent ages of the small-size fractions by about 39% and those of the coarse size fractions by about 46%, which is quite close for significantly different particle sizes. It may be reiterated that although ^{40}Ar diffusion may not be the sole process that decreased the K–Ar apparent ages of fine-clay-size fractions, an alternative addition of K, by itself, is also not a satisfactory explanation of the decrease in the K–Ar apparent ages.

There is an agreement between the calculated curve for the smallest size fraction of 0.125 μm and the reported K–Ar apparent ages, as well as an agreement between the curves for $r=0.21$ and 0.64 μm that approximately overlap the particle-size range of 0.25–1 μm. Furthermore, the estimated diffusion coefficient of ^{40}Ar is low, $D=1.4\times10^{-27}$ cm^2 s^{-1}, but it is of a similar order of magnitude as the diffusion coefficients of Ar in glauconite, phlogopite, and muscovite at about 150 °C, whereas the values extrapolated to 25 °C are much lower (from data in Freer, 1981; Lerman, 1988; Wijbrans and McDougall, 1986). However, we believe that an agreement between the simple model of ^{40}Ar production and concomitant loss, as shown in Fig. 5 for the Gulf Coast Miocene clays and for other formations not plotted here, may be fortuitous, for the following reasons. The depositional Miocene age of the clays is less than 25 Ma, whereas their $^{40}Ar/^{40}K$ ratios and K–Ar apparent ages are much older, indicating a long geologic history before deposition in the Gulf Coast as Tertiary sediments. It seems unlikely, in the absence of any clear indications to the contrary, that the environment of the clays could have remained such that the ^{40}Ar diffusional loss was not affected during the 190 to 350 Ma of their pre-depositional and post-depositional history. A more realistic scenario is presented in the next section.

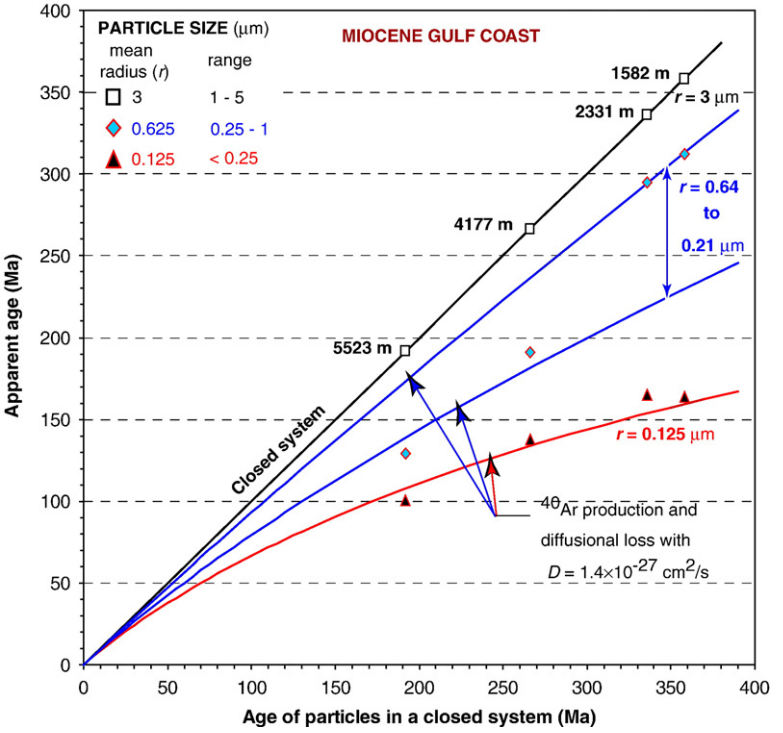

Fig. 5. Calculated $^{40}Ar/^{40}K$ ratios and K–Ar apparent ages of particles (r=0.125 and 0.626 μm) in clay particles at four depths, 1582 to 5523 m (Perry, 1974; see text and Table B.1). Production and diffusional loss of ^{40}Ar from Eq. (A.9), Appendix A, for a case of no initial ^{40}Ar concentration in the particles.

4.3. Closed system, loss, and production of ^{40}Ar

Following the discussion in Section 4.1, we apply the three processes — ^{40}Ar growth in a closed system, start of diffusional loss of the accumulated ^{40}Ar at some time, and continuous production and loss of ^{40}Ar from that time on — to the clay sample from the Miocene of the Gulf Coast, sampled at a depth of 2331 m. This sample (Tables 1 and B.1) is at about mid-depth of the range of the four samples available, its K–Ar apparent ages are considerably older than the depositional stratigraphic age, and each sample is represented by the analyses of three different size fractions. The largest size fraction of 2–10 μm has a K–Ar apparent age of 336 Ma and the smallest, <0.5 μm or mean radius 0.125 μm, has a K–Ar apparent age of 165 Ma. The results are shown in Fig. 6.

The closed-system model of clay particles, initially free of ^{40}Ar, begins to lose ^{40}Ar at different times, from 150 Ma after t=0 to 315 Ma that is about 20 Ma before the present apparent age of the largest size fraction, which is realistic considering the known depositional history of the Gulf Coast sedimentary rocks. In a closed system, the small particles of radius 0.125 μm are assumed to have the same age as the larger-size fractions, all fitting the straight line labeled Closed system. The ^{40}Ar loss from each assumed starting time was calculated from Eq. (A.11), by finding the value of the diffusion coefficient D that results in the change of the $^{40}Ar/^{40}K$ ratio from the value shown on the straight line (Closed system) to the reported apparent age of 165 Ma.

It should be noted that the calculated results give a range of D values within one order of magnitude of 10^{-27} cm^2 s^{-1}. The assumed last point of the start of ^{40}Ar loss at 315 Ma is within the time range of sediment deposition in the Gulf Coast sequence, as mentioned earlier in this section. A shorter time of diffusional loss requires a higher value of D, to bring the particle's K–Ar apparent age to the value sought.

The application of the same analysis as discussed above and shown in Fig. 6 to other fine-size fractions of clays from the Neogene of Borneo, Miocene of the Gulf Coast, Triassic of Morocco and Switzerland, and Permian of Germany gives consistent values of the ^{40}Ar diffusion coefficient for spherical particles mostly in the range from 10^{-28} to 10^{-27} cm^2 s^{-1} that are summarized in Table 1. The results in Table 1 also give the particle-size fractions of clays in the different formations, their K–Ar apparent age, and the range of assumed times for the start of the ^{40}Ar loss. It might be noted that the values of D are very similar for particles

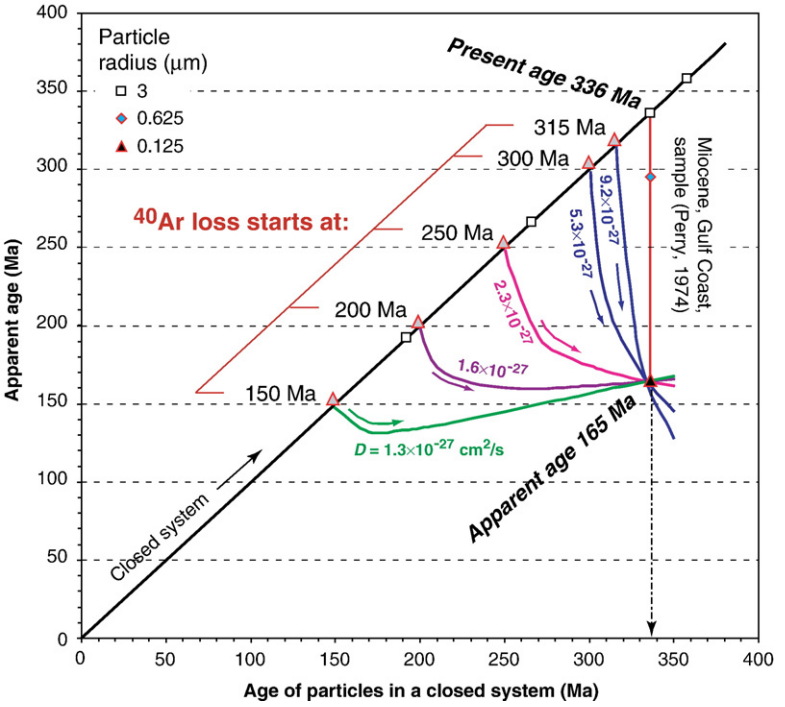

Fig. 6. Simulation of diffusional loss with production of ^{40}Ar in particles of r=0.125 μm, assuming different times for the start of loss (τ=150, 200, 250, 300, and 315 Ma). Clay sample from the U. S. Gulf Coast Miocene (2331 m depth, Table B.1). Model Eq. (A.11), Appendix A.

of different sizes, 0.125 and 0.625 μm, that differ in their volumes by a factor of 125. As discussed under Fig. 4, the values of D for flake-like particles may be higher by a factor of about 5.

The loss of radiogenic ^{40}Ar and consequent lowering of the K–Ar apparent age over some period of time since the start of the process is controlled by the ratio of the diffusion coefficient and particle size, D/r^2 (see Appendix A, Eq. (A.6)). This indicates that the same apparent age would characterize different size fractions if the diffusion coefficient D decreased in proportion to the square of the particle size, r^2. For example, a decrease in the size by a factor of 10 would require a decrease in D by a factor of 100 if the smaller and bigger particles had the same apparent age. An apparent age independent of the particle size would be represented by a horizontal line for the sample plots that are shown in Fig. 3. In the sedimentary formations of different stratigraphic ages (Fig. 3, Table B.1), the K–Ar apparent ages of the smaller-size fractions are pronouncedly lower than the apparent ages of the larger fractions. This suggests that, in terms of a model of ^{40}Ar diffusion with production, the diffusion coefficients of the smaller fractions are relatively greater than they would be in a hypothetical case of a K–Ar apparent age that were the same for all the particle sizes.

5. ^{40}Ar flux from sediments

The release of radiogenic ^{40}Ar from K-containing clays makes the sediments a likely source of some of the ^{40}Ar in the atmosphere, where this isotope is the most abundant constituent (99.6 at.%) of the present-day atmospheric argon. Illite and mixed-layer illite–smectite are the main K-containing clays in sediments. We present below four estimates of the ^{40}Ar flux from continental sediments.

Illite of a synthetic stoichiometric formula $K_{0.6}Al_{2.2}Si_{3.7}O_{10}(OH)_2$ is similar to the rounded-off mean composition that is given by Deer et al. (1962) as $K_{0.6}Al_{2.6}Si_{3.4}O_{10}(OH)_2$, and it may be taken as a representative source of ^{40}Ar in clays of the sedimentary lithosphere. The mass of shales, 0.96×10^{24} g, accounts for 51 wt.% of all the sediments, and illite and mixed-layer illite–smectite have been estimated to represent 56 wt.% of the shales or 0.54×10^{24} g (Li, 2000; Shaw and Weaver, 1965). In addition to the K-bearing clays, shales also contain 4.5 wt.% of K-feldspar of nominal composition $KAlSi_3O_8$ or 0.04×10^{24} g. Potassium represents 4.34 wt.% of the mineral in the illite–smectite solid solution and it represents 14.05 wt.% of the K-feldspar. Using the ^{40}K/K atomic ratio of 1.167×10^{-4} (Steiger

and Jäger, 1977), the masses of ^{40}K in the illites and K-feldspars contained in the shales are:

$$\begin{aligned}&^{40}K \text{ in illites of shales}\\&= 1.67\times10^{-4}\left(5.376\times10^{23}\right.\\&\quad\left.\times\,0.0434\right)/39.1\\&= 6.963\times10^{16}\text{mol}\\&^{40}K \text{ in K-feldspars of shales}\\&= 1.167\times10^{-4}\left(4.32\times10^{22}\right.\\&\quad\left.\times0.1405\right)/39.1\\&= 1.812\times10^{16}\text{ mol.}\end{aligned}$$

Estimate 1. The mass half-age of shales and sandstones is about 600×10^6 years, close to the average mass half-age of all the preserved sediments (Garrels and Mackenzie, 1972). The $^{40}Ar/^{40}K$ ratio of 600 Ma-old minerals would be 0.0414, corresponding to the mass of ^{40}Ar in illite of 2.88×10^{15} mol and in feldspars of 0.75×10^{15} mol. If about 50% of this ^{40}Ar mass escaped from the sediments in 300 Ma by diffusional loss from clays and dissolution of some of the feldspars, as may also be inferred from the range of the ^{40}Ar loss data given in the discussion accompanying Fig. 3, then a mean flux of ^{40}Ar would be:

$$(2.88+0.75)\times10^{15}\times0.5/3\times10^{8}=6\times10^{6}\text{ mol year}^{-1}.$$

The amount of ^{40}Ar lost from sediments, of an order of magnitude of 10^{15} mol, represents only a small fraction of ^{40}Ar in the present-day atmosphere that is about 1.64×10^{18} mol.

Estimate 2. An estimate similar to the preceding is obtained from Eq. (1) that relates the ^{40}Ar concentration in a clay to its K–Ar apparent age, t_{app}. If a decrease in the apparent age, Δt_{app}, is due to a loss of radiogenic argon, $\Delta\,^{40}Ar$, then the rate of ^{40}Ar loss is approximately:

$$\begin{aligned}&\Delta^{40}\text{Ar}/\Delta t_{\text{app}}\approx\lambda_a{}^{40}K\\&=\left(0.581\times10^{-10}\text{ year}^{-1}\right)\left(8.78\times10^{16}\text{ mol}\right)\\&=5\times10^{6}\text{ mol year}^{-1}.\end{aligned}\qquad(6)$$

Estimate 3. A somewhat higher estimate of the ^{40}Ar flux from the sedimentary crust to the atmosphere is obtained from a model of a continuous ^{40}Ar production and release by a first-order flux that is represented by a release-rate parameter ε (Lerman and Clauer, 2005). This release rate is derived from a non-steady-state model of the ^{40}Ar production and escape from illite and mixed-layer illite–smectite in thick sediment sequences (250 to 1800 m), where the $^{40}Ar/^{40}K$ ratio and K–Ar apparent age are nearly constant with depth. A near-constant value of the $^{40}Ar/^{40}K$ ratio with depth mimics a steady-state behavior, which is not the case because the ratios and ages in the sections above and below the constant-age sequence are different. The above defined release-rate parameter ε is obtained from a solution of a mass-balance equation between the production of (^{40}Ar) in particles and its release:

$$d\left(^{40}\text{Ar}\right)/dt=\lambda_a{}^{40}K_0e^{-\lambda t}-\varepsilon\left(^{40}\text{Ar}\right)\qquad(7)$$

where (^{40}Ar) and ^{40}K are the nuclide concentrations in mol g^{-1}. With no initial ^{40}Ar in the particles, the solution of Eq. (7) gives the $^{40}Ar/^{40}K$ ratio as:

$$^{40}\text{Ar}/^{40}\text{K}=\lambda_a\left[1-e^{-(\varepsilon-\lambda)t}\right]/(\varepsilon-\lambda).\qquad(8)$$

The near-constant $^{40}Ar/^{40}K$ ratios and K–Ar apparent ages with depth are not steady-state values because the time to approach a steady state, from Eq. (8), is much longer than the stratigraphic ages of the sedimentary sections.

Sediment sequences of near-constant K–Ar apparent ages occur in the Late Paleozoic (Permian) of North Germany, the Mesozoic sedimentary sequence in the North Sea, the Tertiary of the U. S. Gulf Coast, and the Neogene of Borneo, from which the calculated ^{40}Ar release-rate parameter ε ranges from 3×10^{-9} to 3×10^{-8} $year^{-1}$. For a representative mean age of the clays (Figs. 1 and 3) of about 250 Ma, following the values given in *Estimate 1*, the mass of ^{40}Ar in sediments is about $M_{Ar}=1.4\times10^{15}$ mol ^{40}Ar. From this and a geometric mean of the range of the rate parameter ε, the ^{40}Ar flux from sediments is:

$$1.4\times10^{15}\times9.5\times10^{-9}\approx13\times10^{6}\text{ mol year}^{-1}.$$

Estimate 4. The fourth estimate of the ^{40}Ar flux is based on the diffusion coefficients, as derived in Section 4 and shown in Table 1. If the diffusion of ^{40}Ar occurs at the surface of a spherical particle, over some distance Δh, then the flux from the entire mass of the particles would be:

$$\text{Flux}=(D/\Delta h)\times{}^{40}\text{Ar}\times4\pi r^2N\rho\text{ (mol/year)}\qquad(9)$$

where D is the diffusion coefficient (cm^2/year), Δh is the diffusional distance near the sphere surface (cm), ^{40}Ar is a mean concentration in the particles (mol/g), r is the particle radius (cm), N is the number of particles of this radius in the sediment, and ρ is the particle density (g/cm^3). In the same notation as in Eq. (9), the mass of ^{40}Ar in the particles is:

$$M_{\text{Ar}}={}^{40}\text{Ar}\times(4/3)\pi r^3N\rho\text{ (mol)}.\qquad(10)$$

Substitution of Eq. (10) in Eq. (9) gives:

$$\text{Flux} = (D/\Delta h) \times 3M_{\text{Ar}}/r \text{ (mol/year)}. \quad (11)$$

A representative value of D from Table 1 is about 1×10^{-27} cm^2/s or 3×10^{-20} cm^2/year. For the thickness of the diffusional layer in the particle, we assume a distance comparable to the unit cell dimension of 5 to 10 Å (Section 4.1), the mass of ^{40}Ar of about 1.4×10^{15} mol, as given in the preceding estimate, and representative particle radius of 1 to 5 μm. Using these values, the ^{40}Ar flux from Eq. (11) is bracketed by the following:

$$\text{Flux} = \frac{3\times10^{-20}\ \text{cm}^2/\text{year}}{(5\text{ to }10)\times10^{-8}\ \text{cm}} \cdot \frac{3\times1.4\times10^{15}\ \text{mol}}{(1\text{ to }5)\times10^{-4}\ \text{cm}}$$

$$= 5 \text{ to } 13\times10^{6}\ \text{mol/year}.$$

The four preceding estimates of the ^{40}Ar flux from sediments to the atmosphere are close one to another, but they are smaller than the flux from the continental crust, estimated by Allègre et al. (1986) as 34×10^6 mol/year. It is to be expected that the ^{40}Ar flux from sediments would be smaller than the flux from the continental crust because the mass of the crust is much greater, whereas their mean K concentrations are comparable, 1.78 and 1.50 wt.%, respectively (Li, 2000; Rudnick and Gao, 2003). The mass of the shales (0.96×10^{24} g), as the main sedimentary source of the ^{40}Ar release to the atmosphere, is also several-fold smaller than the mass of only the upper continental crust, 9×10^{24} g, extending to 19 km depth (Wedepohl, 1995) and over the surface area of the present-day continents and continental shelves (177×10^6 km^2). The K concentration in shales, 2.51 wt.% K, is comparable to that in the upper continental crust, 2.32 to 2.60 wt.%, where K occurs primarily in feldspars (Li, 2000; Rudnick and Gao, 2003), but the generally higher temperatures in the continental crust may be responsible for a stronger ^{40}Ar flux to the atmosphere.

6. Summary and conclusions

An analysis of older and newer data from sediments of the Cambrian to Neogene age confirms and expands the well-known observation that the K–Ar apparent ages of fine-clay particles in the Mesozoic and Tertiary formations can be much older than their depositional stratigraphic ages, indicating that clays had a long geologic history before deposition. The discrepancies between the K–Ar apparent ages and stratigraphic ages are also discussed as being possibly due to such geochemical mechanisms as: (a) ^{40}Ar release from clay particles making their apparent ages younger than the stratigraphic age; (b) diagenetic addition of K to the minerals without loss or with limited loss of ^{40}Ar that also lowers their apparent age, but for which no sufficiently extensive data exist; and (c) selective removal of ^{40}K or (d) addition of radiogenic Ar to clays. However, selective removal of ^{40}K is considered unlikely and a possible addition of ^{40}Ar to sedimentary clays not significant. Furthermore, the calculated lowering of the K–Ar apparent age of clay particles may be very similar when it is based on models of two very different processes: either by addition of K without loss of ^{40}Ar or by production of ^{40}Ar and its concomitant diffusional loss from the particles.

The clays of Cambrian to Neogene ages show that their K–Ar apparent ages decrease from the larger to the smallest size fraction and that the magnitude of the decrease varies depending on the different ages and particle-size range of the samples. The linear dimensions of clay particles in the studied samples vary from the smallest to the largest size by a factor of about 10 to 100. The decrease in the apparent age is represented by the slope of a linear fit to the values of the K–Ar apparent age as a function of the particle size, where a steeper slope indicates a greater fraction of ^{40}Ar lost. The estimated mass fractions of the ^{40}Ar lost from the smaller particles relative to the larger sizes vary from a low loss of 13±6% in the Paleozoic and Mesozoic formations to as much as 39±5% in the younger, Neogene formations, where the particle-size range is a factor of 10. Higher percentage losses apply to the particle assemblages where the smallest size is <0.1 of the largest particles. The less steep slopes of the plotted regression lines and correspondingly smaller fractions of escaped ^{40}Ar in the geologically older formations may be in part accounted for by the closure of the ^{40}Ar escape in the clay-sediment systems in the past.

In the sedimentary suite from the Neogene Mahakam basin (Eastern Borneo), in clays of depositional age <18 Ma, it could be shown that older detrital components are mixed with authigenic illite-type material in the smallest size fractions. Estimated mass fractions of the authigenic illite increase with the depositional age or depth in the sedimentary sequence, from about 22 to 38%.

A model of diffusional loss of ^{40}Ar from clays (or other K-bearing minerals), approximated to particles of such shapes as spheres, cylinders, or flakes, is often used in laboratory studies and interpretation of natural occurrences of the lowering of ^{40}Ar/^{40}K ratios and K–Ar apparent ages. A deficiency of this generic model is that it does not take into account the continuous production of ^{40}Ar

during the time of escape that may be geologically long and may contribute significantly to the ^{40}Ar content of the particles. A model of ^{40}Ar production and simultaneous escape in particles in the shapes of a sphere and a flake (slab), where diffusional transport occurs only across a smaller surface area of two parallel surfaces, as opposed to the whole surface of a sphere, has been discussed in detail. An analysis, based on this production and simultaneous escape model, of fine-clay fractions in Neogene sediments that are known not to have been subjected to strong thermal events and in Paleozoic sediments, some of which might have been subjected either to abnormal geothermal gradients or to migrations of hot fluids as shown by fluid-inclusion microthermometry, gives ^{40}Ar diffusion coefficients consistently in a range from 10^{-28} to 10^{-27} cm^2/s. The order of magnitude of such values is comparable to the diffusion coefficients in sheet-structured silicates near 150 °C, as derivable from data reported in the literature, but not related either to normal burial, abnormal geothermal gradient, or migration of hot fluids.

Illite and mixed-layered illite–smectite of shales are the main K-containing clay minerals in the sedimentary crust. Estimates of the ^{40}Ar flux from the sediments to the atmosphere, based on the results reported in this paper, give values from 5×10^6 to 13×10^6 mol ^{40}Ar/year. These values, as may be expected, are lower than the ^{40}Ar flux from the continental crust, as estimated by other investigators, and they depend on the estimates of the ^{40}Ar mass fraction that escaped from clays during the 300 to 600 Ma period of sediment deposition and recycling.

Acknowledgements

This research was supported by the Arthur L. Howland Fund of the Department of Earth and Planetary Sciences, Northwestern University, ANDRA (Agence Nationale pour la gestion des déchets nucléaires), the French agency in charge of nuclear waste disposal, and NSF grant EAR02-23509. We are grateful to two anonymous reviewers and Associate Editor Lynn M. Walter for their insightful comments on an earlier version of this paper, which helped us improve it. This is publication No. 2007.301 of Ecole et Observatoire des Sciences de la Terre (EOST), Université Louis Pasteur, Strasbourg.

Appendix A

A.1. Simple relationships

The radioactive decay of ^{40}K to ^{40}Ar, in a closed system that contained initially no ^{40}Ar and where neither ^{40}K nor ^{40}Ar are added or lost, produces the following relationship for the ^{40}Ar/^{40}K concentration ratio as a function of time:

$$\frac{^{40}\mathrm{Ar}}{^{40}\mathrm{K}} = \frac{\lambda_a}{\lambda}\left(e^{\lambda t} - 1\right). \tag{A.1}$$

The concept of an apparent age (Faure, 1986) of a K- and Ar-containing mineral represents the cases where the ^{40}K and ^{40}Ar concentrations may differ from those in a closed system. The apparent age, t_{app}, of a particle initially free of ^{40}Ar is from the preceding:

$$t_{app} = \frac{1}{\lambda}\ \ln\left(1 + \frac{\lambda}{\lambda_a}\frac{^{40}\mathrm{Ar}}{^{40}\mathrm{K}}\right) \tag{A.2a}$$

where $\lambda = 5.543\times10^{-10}$ year^{-1} is the total decay constant of ^{40}K (that is, its rate of decay to ^{40}Ar and ^{40}Ca) and $\lambda_a = 0.581\times10^{-10}$ year^{-1} is the ^{40}K decay rate constant to ^{40}Ar (Steiger and Jäger, 1977).

An approximation valid for the apparent ages up to 200 to 300 Ma:

$$t_{app} \approx \frac{1}{\lambda_a}\frac{^{40}\mathrm{Ar}}{^{40}\mathrm{K}}. \tag{A.2b}$$

In a system where potassium is added at a linear rate of a year^{-1} or removed at a rate $-a$, $^{40}\mathrm{K} = {}^{40}\mathrm{K}_0(1\pm at)$, but where no ^{40}Ar is added or lost, the ^{40}Ar/^{40}K ratio is:

$$\frac{^{40}\mathrm{Ar}}{^{40}\mathrm{K}} = \frac{\lambda_a}{\lambda(1+at)}\left[\left(1+\frac{a}{\lambda}\right)e^{\lambda t} - \left(1+at+\frac{a}{\lambda}\right)\right] \tag{A.3}$$

where a can be either positive or negative. With $a=0$, the preceding equation is identical to that for the closed system, Eq. (A.1).

A.2. ^{40}Ar diffusional loss from spherical particles

Extensive treatment of the mathematical models of production and diffusional escape of ^{40}Ar in clay and other mineral particles can be found, for example, in the references cited in the text of Section 1. More general derivations of the mathematical relationships that apply to different physical, chemical, and geological radionuclide systems have been given by Carslaw and Jaeger (1959), Crank (1967), and Wasserburg (1954, 1963).

A.2.1. Diffusional loss without production

The loss of ^{40}Ar from a spherical particle is usually represented in the literature as the fraction of ^{40}Ar lost (f), starting at some time $t=0$, in the following form:

$$f = 1 - \frac{6}{\pi^2}\sum_{n=1}^{\infty}\frac{\exp\left(-n^2\pi^2 Dt/r^2\right)}{n^2}. \quad (A.4)$$

The atomic ratio $R=^{40}\mathrm{Ar}/^{40}\mathrm{K}$ that remains in the particle after the ^{40}Ar diffusional escape started at time $t=\tau$ is:

$$R = \frac{6\lambda_a}{\lambda\pi^2}\cdot\left(e^{\lambda\tau}-1\right)\cdot\sum_{n=1}^{\infty}\frac{e^{-n^2\beta\lambda(t-\tau)}}{n^2} \quad (A.5)$$

where the diffusion release of ^{40}Ar started at time $t=\tau$, and β is a dimensionless parameter that depends on the diffusion coefficient D, particle radius r, and the decay rate constant of ^{40}K λ:

$$\beta = \frac{D\pi^2}{\lambda r^2}. \quad (A.6)$$

Parameter β appears in other equations given in this Appendix, that describe the production and simultaneous diffusion of ^{40}Ar out of spherical and flake-like particles. This parameter determines the ^{40}Ar/^{40}K ratio and K–Ar apparent age of a particle where diffusion and simultaneous production occurred over some period of time $t-\tau$. For particles of different sizes to have the same apparent age, the value of β should be the same, which requires the ratio D/r^2 to remain constant for different size fractions. This in turn implies that a smaller apparent age of a smaller-size fraction may be explained by a relatively higher value of D than in a case of the apparent age being independent of the particle size.

Eq. (A.5) does not take into account the production of radiogenic ^{40}Ar after the start of its escape from the particle. The initial ^{40}Ar/^{40}K ratio at time $t=\tau$ is from Eq. (A.5):

$$R_0 = \frac{\lambda_a}{\lambda}\cdot\left(e^{\lambda\tau}-1\right). \quad (A.7)$$

A.2.2. ^{40}Ar production and loss from zero initial concentration

An equation for the temperature in a spherical particle, of radius $0<x<r$ and zero initial temperature, where heat is produced at a rate that declines exponentially with time, $A_0e^{-\lambda t}$, is given by Carslaw and Jaeger (1959, p. 245). This equation can be adopted for the production of ^{40}Ar at the decay rate of ^{40}K, $\lambda_a{}^{40}\mathrm{K}_0e^{-\lambda t}$, in a particle initially free of ^{40}Ar, that gives the ^{40}Ar concentration in the particle as a function of the radial distance from the center and time $C(x,t)$. A mean concentration of ^{40}Ar in the particle of radius r is obtained by integration of $C(x,t)$ and division by the particle volume:

$$\left(^{40}\mathrm{Ar}\right) = \frac{3}{4\pi r^3}\int_0^r 4\pi x^2 C(x,t)dx. \quad (A.8)$$

A mean ^{40}Ar/^{40}K ratio R in such a particle is:

$$R = \frac{3\lambda_a\beta}{\lambda\pi^2} - \frac{3\lambda_a\beta^{1/2}\cot\left(\pi/\beta^{1/2}\right)}{\lambda\pi} - \frac{\lambda_a}{\lambda} - \frac{6\lambda_a}{\lambda\pi^2}\cdot\sum_{n=1}^{\infty}\frac{e^{-\left(n^2\beta-1\right)\lambda(t-\tau)}}{n^2\left(n^2\beta-1\right)} \quad (A.9)$$

where the dimensionless parameter β is defined in Eq. (A.6). The first three terms in Eq. (A.9) are constants, for any given values of the diffusion coefficient D and particle radius r. However, in the last term, the summation series converges only if the following inequality is obtained: $n^2\beta-1>0$. A more restrictive condition for the first term in the summation, at $n=1$, is:

$$D\pi^2/r^2>\lambda. \quad (A.10)$$

A physical significance of the latter condition is that the diffusion coefficient must be sufficiently large and diffusional flux out sufficiently fast relative to the particle size where the diffusing species is produced at a rate determined by λ. If this is not the case, then the ^{40}Ar produced would not be removed sufficiently fast from the particle.

Mathematically, Eq. (A.9) of ^{40}Ar production and escape leads to a steady state, when the term $\sum$ approaches zero. This leaves the three first terms that do not depend on time. Their sum, depending on D and particle size, gives a constant ^{40}Ar/^{40}K value in each case, which might be interpreted as a steady-state apparent age. However, as the concentration of ^{40}K decreases with a long half-life of 1.25×10^9 years or about 0.5% every 10^7 years, a hypothetical steady state would be approached after periods of time that may be far beyond those considered in the examples discussed in this paper.

Combination of the conditions in Eq. (A.5), describing the escape of ^{40}Ar accumulated up to time $t=\tau$, and Eq. (A.9) that describes the ^{40}Ar new production at time

$t>\tau$, gives the following equation that was used to compute the curves shown in Figs. 4 and 6:

$$\frac{^{40}\mathrm{Ar}}{^{40}\mathrm{K}} = \overbrace{\frac{6\lambda_a}{\lambda\pi^2}\cdot\left(e^{\lambda\tau}-1\right)\cdot\sum_{n=1}^{\infty}\frac{e^{-n^2\beta\lambda(t-\tau)}}{n^2}}^{^{40}\mathrm{Ar\ diffusion\ out,\ starting\ at\ time}\ t=\tau} + \frac{3\lambda_a\beta}{\lambda\pi^2} - \frac{3\lambda_a\beta^{1/2}\cot\left(\pi/\beta^{1/2}\right)}{\lambda\pi} - \frac{\lambda_a}{\lambda} - \overbrace{\frac{6\lambda_a}{\lambda\pi^2}\cdot\sum_{n=1}^{\infty}\frac{e^{-\left(n^2\beta-1\right)\lambda(t-\tau)}}{n^2\left(n^2\beta-1\right)}}^{^{40}\mathrm{Ar\ production\ and\ diffusion\ out,\ starting\ at\ time}\ t=\tau}. \quad (A.11)$$

A.3. ^{40}Ar diffusional loss from flake-shaped particles

In a flake or slab, diffusion occurs across two parallel planes, as was discussed in the text of Section 4.1. Mathematically, a flake is characterized by a certain thickness or distance between the two parallel planes, but it is not limited in the other two dimensions. In our treatment, the flake is taken as a particle with the distance between the two planes (x) across which diffusion takes place as equal to the diameter ($2r$) of a spherical particle ($-r<x<r$).

A.3.1. Diffusional loss without production

The ^{40}Ar/^{40}K ratio R in a flake of half-thickness r follows from the equation for the ^{40}Ar fraction lost by diffusion, without additional production, that is given in the references cited in the text of Section 1 and Carslaw and Jaeger (1959, p. 97):

$$R = \frac{8\lambda_a}{\lambda\pi^2}\cdot\left(e^{\lambda\tau}-1\right)\cdot\sum_{n=1}^{\infty}\frac{e^{-\left[(2n-1)^2\beta/4-1\right]\lambda(t-\tau)}}{(2n-1)^2} \quad (A.12)$$

where the initial ratio $R_0=(^{40}\mathrm{Ar}/^{40}\mathrm{K})_0$ at time $t=\tau$ is as given in Eq. (A.7) and dimensionless β in Eq. (A.6).

A.3.2. ^{40}Ar production and loss from zero initial concentration

A mean ^{40}Ar/^{40}K ratio in a flake-shaped particle, where no ^{40}Ar is present initially and it is produced at an exponentially declining rate of $\lambda_a{}^{40}\mathrm{K}_0e^{-\lambda t}$, can be derived from the equation given by Carslaw and Jaeger (1959, p. 132) for a concentration change, $C(x,t)$, along the linear dimension between the two parallel surfaces, $-r<x<r$. A mean concentration of ^{40}Ar in a flake is:

$$\left(^{40}\mathrm{Ar}\right) = \frac{1}{2r}\int_{-r}^{r}C(x,t)dx. \quad (A.13)$$

Following the integration procedure described in Section A.2.2 above:

$$R = \frac{\lambda_a\ \tan\left(\pi/\beta^{1/2}\right)}{\pi\beta^{1/2}} - \frac{\lambda_a}{\lambda} - \frac{8\lambda_a}{\lambda\pi^2} \times\sum_{n=1}^{\infty}\frac{e^{-\left[(2n-1)^2\beta/4-1\right]\lambda(t-\tau)}}{(2n-1)^2\left[(2n-1)^2\beta/4-1\right]}. \quad (A.14)$$

Combination of the conditions in Eq. (A.12), describing the escape of ^{40}Ar accumulated up to time $t=\tau$, and Eq. (A.14) that describes the ^{40}Ar new production and escape at time $t>\tau$, gives the following equation that was used to compute the curves for a flake shown in Fig. 4B,C:

$$R = \overbrace{\frac{8\lambda_a}{\lambda\pi^2}\cdot\left(e^{\lambda\tau}-1\right)\cdot\sum_{n=1}^{\infty}\frac{e^{-\left[(2n-1)^2\beta/4-1\right]\lambda(t-\tau)}}{(2n-1)}}^{^{40}\mathrm{Ar\ diffusion\ out,\ starting\ at\ time}\ t=\tau} + \frac{\lambda_a\tan\left(\pi/\beta^{1/2}\right)}{\pi\beta^{1/2}} - \frac{\lambda_a}{\lambda} - \overbrace{\frac{8\lambda_a}{\lambda\pi^2}\cdot\sum_{n=1}^{\infty}\frac{e^{-\left[(2n-1)^2\beta/4-1\right]\lambda(t-\tau)}}{(2n-1)^2\left[(2n-1)^2\beta/4-1\right]}}^{^{40}\mathrm{Ar\ production\ and\ diffusion\ out,\ starting\ at\ time}\ t=\tau} \quad (A.15)$$

Appendix B. Supplementary data

Supplementary data associated with this article can be found, in the online version, at doi:10.1016/j.chemgeo.2007.05.014.

References

Allègre, C.J., Staudacher, T., Sarda, P., 1986. Rare gas systematics: formation of the atmosphere, evolution and structure of the Earth's mantle. Earth and Planetary Science Letters 81, 127–150.

Aronson, J.L., Hower, J., 1976. Mechanism of burial metamorphism of argillaceous sediments: 2. Radiogenic argon evidence. Geological Society of America Bulletin 87, 738–744.

Aylmore, L.A.G., 1974. Gas sorption in clay mineral systems. Clays and Clay Minerals 22, 175–183.

Bachman, L.J., Krantz, D.E., Böhlke, J., 2002. Hydrogeologic Framework, Ground-water Geochemistry, and Assessment of Nitrogen Yield from Base Flow in Two Agricultural Watersheds, Kent County, Maryland. U. S. Environmental Protection Agency, National Risk Management Research Laboratory, Cincinnati, Ohio. EPA/600/R-02/008.

Biagi, P.F., Piccolo, R., Minafra, A., Maggipinto, T., Castellana, L., Molchanov, O., Ermini, A., Capozzi, V., Perna, G., Khatkevich, Y.M., Gordeev, E.I., 2004. Retrospective analysis for detecting seismic

precursors in groundwater argon content. Natural Hazards and Earth System Sciences 4, 9–15.
Carslaw, H.S., Jaeger, J.C., 1959. Conduction of Heat in Solids, 2nd edit. Oxford Univ. Press, x+520 pp.
Chaudhuri, S., Środoń, J., Clauer, N., 1999. K–Ar dating of illitic fractions of Estonian "Blue Clay" treated with alkylammonium cations. Clays and Clay Minerals 47, 96–102.
Chen, C.T.A., 2006. General chemistry of seawater. Our Fragile World: Challenges and Opportunities for Sustainable Development, Encyclopedia of Life Support Systems (EOLSS), Developed Under the Auspices of the UNESCO. Eolss Publishers, Oxford, U. K. [http://www.eolss.net] http://mgac.nsysu.edu.tw/ctchen/Publications/A/2006/205.pdf.
Clauer, N., 2005. Determinations of ^{40}Ar in the pore space of argillites. Unpublished results.
Clauer, N., 2006. Towards an isotopic modeling of the illitization process based on data of illite-type fundamental particles from mixed-layer illite–smectite. Clays and Clay Minerals 54, 116–127.
Clauer, N., Chaudhuri, S., 1995. Clays in Crustal Environments. Isotope Dating and Tracing. Springer Verlag, Heidelberg, 358 pp.
Clauer, N., Chaudhuri, S., 2001. Extracting K–Ar ages from shales: the analytical evidence. Clay Minerals 36, 227–235.
Clauer, N., Środoń, J., Franců, J., Šucha, V., 1997. K–Ar dating of illite fundamental particles separated from illite/smectite. Clay Minerals 32, 181–196.
Clauer, N., Zwingmann, H., Gorokhov, I.M., 2003. Post-depositional evolution of platform claystones based on a simulation of thermally induced diffusion of radiogenic ^{40}Ar from diagenetic illite. Journal of Sedimentary Research 73, 58–63.
Clauer, N., Rousset, D., Środoń, J., 2004. Modeled shale and sandstone burial diagenesis based on the K–Ar systematics of illite-type fundamental particles. Clays and Clay Minerals 52, 576–588.
Crank, J., 1967. The Mathematics of Diffusion, 2nd edit. Oxford Univ. Press, vi+347 pp.
Cascarini de Torre, L.E., Fertitta, A.E., Flores, E.S., Llanos, J.L., Bottani, E.J., 2004. Characterization of shungite by physical adsorption of gases. Journal of the Argentine Chemical Society 92 (4/6), 51–58.
Deer, W.A., Howie, R.A., Zussman, J., 1962. Rock-forming Minerals, Vol. 3, Sheet Silicates. Longmans, London. x+ 270 pp.
Dodson, M.H., 1973. Closure temperature in cooling geochronological and petrological systems. Contributions to Mineralogy and Petrology 40, 259–274.
Drever, J.I., 1997. The Geochemistry of Natural Waters, 3rd edit. Prentice-Hall, Upper Saddle River, N. J., xii+388 pp.
Faure, G., 1986. Principles of Isotope Geology, 2nd edit. Wiley, New York, xv+589 pp.
Freer, R., 1981. Diffusion in silicate minerals and glasses: a data digest and guide to literature. Contribution to Mineralogy and Petrology 76, 440–454.
Furlan, S., 1994. Transferts de matière au cours de la diagenèse d'enfouissement dans le bassin du delta de la Mahakam (Indonésie). Un nouveau concept pour le mécanisme de l'utilisation. Thèse de Doctorat, Université Louis Pasteur, Institut de Géologie, Strasbourg, 224 pp.
Furlan, S., Clauer, N., Chaudhuri, S., Sommer, F., 1996. K transfer during burial diagenesis in the Mahakam Delta Basin (Kalimantan, Indonesia). Clays and Clay Minerals 44, 157–169.
Gaines Jr., G.L., 1958. The adsorption of gases on ion exchanged mica. II. Thermodynamics of rare gas adsorption. Journal of Physical Chemistry 62, 1526–1530.
Gaines Jr., G.L., Rutkowski, C.P., 1958. The adsorption of gases on ion-exchanged mica. I. Argon and krypton isotherms and BET surface area measurements. Journal of Physical Chemistry 62, 1521–1525.
Garrels, R.M., Mackenzie, F.T., 1972. A quantitative model for the sedimentary rock cycle. Marine Chemistry 1, 27–41.
Glasmann, J.R., Larter, S., Briedis, N.A., Lundegard, P.D., 1989. Shale diagenesis in the Bergen High Area, North Sea. Clays and Clay Minerals 37, 97–112.
Hamme, R.C., Emerson, S.R., 2004. The solubility of neon, nitrogen and argon in distilled water and seawater. Deep-Sea Research I 51, 1517–1528.
Heaton, T.H.E., Vogel, J.C., 1981. "Excess air" in groundwater. Journal of Hydrology 50, 201–216.
Honty, M., Uhlík, P., Šucha, V., Čaplovičová, M., Franců, J., Clauer, N., Biroň, A., 2004. Smectite-to-illite alteration in salt-bearing bentonites (the East Slovak Basin). Clays and Clay Minerals 52, 533–551.
Hunziker, J.C., 1986. The evolution of illite to muscovite: an example of the behavior of isotopes in low-grade metamorphic terrains. Chemical Geology 57, 31–40.
Hunziker, J.C., Frey, M., Clauer, N., Dallmeyer, R.D., Friedrichsen, H., Flehmig, W., Hochstrasser, K., Roggwiler, P., Schwander, H., 1986. The evolution of illite to muscovite: mineralogical and isotopic data from the Glarus Alps, Switzerland. Contributions to Mineralogy and Petrology 92, 157–180.
Huon, S., Cornée, J.J., Piqué, A., Rais, N., Clauer, N., Liewig, N., Zayane, R., 1993. Mise en évidence au Maroc d'événements thermiques d'âge triasico-liasique liés à l'ouverture de l'Atlantique. Bulletin Société Géologique de France 164, 165–176.
Lerman, A., 1988. Geochemical Processes — Water and Sediment Environments. Wiley, New York. (Reprint edit., R. E. Krieger, Malabar, Fla.), viii+481 pp.
Lerman, A., Clauer, N., 2005. Loss of radiogenic ^{40}Ar in the fine-clay size fractions of sediments. Clays and Clay Minerals 53, 234–249.
Li, Y.H., 2000. A Compendium of Geochemistry. Princeton Univ. Press, Princeton, N. J., xiv+475 pp.
McDougall, I., Harrison, T.M., 1999. Geochronology and Thermochronology by the ^{40}Ar/^{39}Ar method, 2nd edit. Oxford Univ. Press, New York, 269 pp.
Neimark, A.V., 2001. New Method for Zeolites Characterization. TRI/Princeton, Princeton, N. J., 4 pp., http://www.yuasa-ionics.co.jp/tec/pdf/etc/zeolite_lette_032901r1.pdf.
Perry Jr., E.A., 1974. Diagenesis and the K–Ar dating of shales and clay minerals. Geological Society of America Bulletin 85, 827–830.
Rudnick, R.L., Gao, S., 2003. Composition of the continental crust. In:. Holland, H.D., Turekian, K.K. (Eds.), Treatise on Geochemistry, vol. 3 (Drever, J.I., Ed.). Elsevier, Amsterdam, pp. 1–64.
Saito, A., Foley, H.C., 1995. High-resolution nitrogen and argon adsorption on ZSM-5 zeolites: effects of cation exchange and Si/Al ratio. Microporous Materials 3, 543–556.
Sayed Hassan, M., Villiéras, F., Razafitianamaharavo, A., Michot, L.J., 2005. Role of exchangeable cations on geometrical and energetic surface heterogeneity of kaolinites. Langmuir 21, 12283–12289.
Schaltegger, U., Zwingmann, H., Clauer, N., Larqué, P., Stille, P., 1995. K–Ar dating of a Mesozoic hydrothermal activity in Carboniferous to Triassic clay minerals of northern Switzerland. Schweizerische Mineralogische und Petrographische Mitteilungen 75, 163–176.
Shannon, R.D., 1976. Revised effective ionic radii and systematic studies of interatomic distances in halides and chalcogenides. Acta Crystallographica A 32, 751–767.
Shaw, D.B., Weaver, C.E., 1965. The mineralogical composition of shales. Journal of Sedimentary Petrology 35, 213–222.

Steiger, R.H., Jäger, E., 1977. Subcommission on geochronology: convention on the use of decay constants in geo- and cosmochronology. Earth and Planetary Science Letters 36, 359–362.

Šucha, V., Kraus, I., Gerthofferova, H., Petes, J., Serekova, M., 1993. Smectite to illite conversion in bentonites and shales of the East Slovak Basin. Clay Minerals 28, 243–253.

Thommes, M., Smarsly, B., Groenewolt, M., Ravikovitch, P.I., Neimark, A.V., 2006. Adsorption hysteresis of nitrogen and argon in pore networks and characterization of novel micro- and mesoporous silicas. Langmuir 22, 756–764.

Tournassat, C., Neaman, A., Villiéras, F., Bosbach, D., Charlet, L., 2003. Nanomorphology of montmorillonite particles: estimation of the clay edge sorption site density by low-pressure gas adsorption and AFM observations. American Mineralogist 88, 1989–1995.

Turner, G., 1968. The distribution of potassium and argon in chondrites. In: Ahrens, L.H. (Ed.), Origin and Distribution of the Elements. Pergamon Press, Oxford, pp. 387–398.

Wasserburg, G.J., 1954. Argon^{40}:potassium^{40} dating. In: Faul, H. (Ed.), Nuclear Geology; A Symposium on Nuclear Phenomena in the Earth Sciences. Wiley, New York, pp. 341–349.

Wasserburg, G.J., 1963. Diffusion processes in lead–uranium systems. Journal of Geophysical Research 68, 4823–4846.

Wedepohl, H.K., 1995. The composition of the continental crust. Geochimica et Cosmochimica Acta 59, 1217–1232.

Wijbrans, J.R., McDougall, I., 1986. $^{40}Ar/^{39}Ar$ dating of white micas from an Alpine high-pressure metamorphic belt of Naxos (Greece): the resetting of the argon isotopic system. Contributions to Mineralogy and Petrology 93, 187–194.

Zwingmann, H., 1995. Study of the Conditions of Gas Emplacement in Sandstone Reservoirs (Rotliegende of Germany). Mineralogical, Morphological, Geochemical and Isotopical Aspects. Doctoral Thesis, Université Louis Pasteur, Institut de Géologie, Strasbourg, 210 pp.